AIAA SciTech Forum
8-12 January 2024, Orlando, FL
AIAA SCITECH 2024 Forum

10.2514/6.2024-1004

Stochastic Model for Electrical Properties of Inkjet Printed Carbon Nanotube Films

Samarth Motagi[1] and Sirish Namilae[2]*
Embry-Riddle Aeronautical University, Daytona Beach, FL, 32114, USA

Inkjet-printing of carbon nanotube (CNT) films results in distinct microstructural characteristics and corresponding electrical behaviors. These films typically exhibit increased conductivity with increasing number of layers, higher alignment in the print direction, and unique microstructures corresponding to sessile drop and twin-line deposition phenomenon. In this study, a stochastic percolation model was used to investigate the effects of electrical conductivity and resistance on layer-wise inkjet-printed carbon nanotubes. The model was employed to generate microstructures, enabling a parametric exploration of the ink composition, alignment, and agglomeration of CNTs within printed structures affect the sheet resistance with respect to the number of printed layers. A high degree of CNT alignment hindered CNT network formation, resulting in higher resistivity, whereas the partial alignment lowered the network resistivity. The effect of the unique microstructural features developed due to printing on the electrical behavior is discussed.

I. Nomenclature

l_i	=	length of CNT
$\emptyset_i$	=	polar angle
n	=	number of layers
t	=	distance between each layer
P	=	Percolation probability
n_p	=	number of microstructures with at least one conductive path
N	=	total number of microstructures
ξ_{agg}	=	agglomeration level
α_{agg}	=	agglomeration angle

II. Introduction

Extended space missions face notable challenges in obtaining necessary replacement parts for repair and maintenance, and new components for future missions. For example, critical circuitry essential for International Space Station (ISS) operations must either be pre-stored or transported from earth, resulting in significant time delays and logistical complications. Capability to manufacture parts and equipment in the space environment could provide a solution to circumvent these constraints. 3D printing has emerged as a transformative tool with unparalleled potential for manufacturing in the space environment. In recent years, the importance of 3D printing in space has gained significant attention for applications, including structures such as circuits [1], sensors [2], solar cells [3], tissue engineering [4], surgical resources [5], and even food production [6]. The feasibility of 3D printing in space has been demonstrated with the successful creation of the first printed component: a faceplate for the extruder casing, produced while in orbit [7].

Inkjet printing has gained a lot of attention in recent years for layer-by-layer printing of multilayer parts and 3D electrical circuits. The non-contact manufacturing feature of inkjet printing has resulted in an efficient method for printing thin films of electrical circuit lines and patterned electrodes on flexible substrates [8]. Other appealing aspects of this technique include decreased material waste, low cost, and scalability to large-scale manufacturing. Inkjet

[1] Ph.D. Student, Aerospace Engineering, Email: motagis@my.erau.edu
[2] Professor, Aerospace Engineering, Email: namilaes@erau.edu (*Corresponding Author).

printing has been successfully applied for fabrication of organic transistors [9], light-emitting diodes [10], biopolymer arrays [11], solar cells [12] and fuel cells [13].

The primary challenges in most ink formulations are (a) achieving adequate dispersion state and (b) obtaining long-term stability of the ink or shelf life [14][15]. Due to the van der Waals attraction and Coulomb forces between the nanoparticles, CNT ink is difficult to disperse uniformly in the solvent. The agglomeration of CNT films deteriorates the electrical properties because of microscopic inhomogeneity [16]. During inkjet printing, CNTs may gather at the periphery, causing a coffee ring effect that creates an uneven film and an unstable resistance [17].

Many studies have demonstrated that aligning the CNTs in an appropriate orientation can boost electron mobility [18][19][20] and reduce the quantity of CNT content to form a conducting percolation network. Compared with the random alignment of CNT, aligned CNT exhibit improved mechanical and thermal characteristics [21]. To alter the orientation of CNTs, a driving torque is required, which can be applied through electrical, magnetic or mechanical means [22]. Several recent studies have used inkjet printing to achieve CNT alignment. Beyer et al. [23] devised a method for arbitrarily increasing the concentration of deposited material by matching the deposition and evaporation rates during inkjet printing, and they utilized it to enhance the liquid crystalline behavior of CNTs in suspension. By removing the layers using elastomeric peeling process, the bulk morphology of these films revealed stacked planar layers, indicating sematic ordering. Beard et al. [24] used inkjet printing to successfully produce patterned vertically aligned carbon nanotube.

Inkjet printing relies on the notion of evaporation-driven nanoparticle self-assembly. During the evaporation process of elongated particles such as carbon nanotubes, the shear force acting on their 1-dimensional structure causes nanotubes to align along the contact line [21]. If an accelerated evaporation rate at the liquid-substrate interface is observed, then CNTs agglomerate along the liquid edge owing to convective flow, resulting in the "coffee-ring" effect. To examine the particle alignment and orientation of CNTs, several experiments on sessile drop [21][25][26][27] and the twin-line deposition concept [17][28][29] have been conducted.

Computational modeling can elucidate the effect of microstructural features, alignment and agglomeration on electrical and thermomechanical behaviors of CNT networks. Many modeling approaches have been used for this purpose. Jamin et al. [30] adopted a computational micromechanics approach to measure the effective thermal and electrical conductivity of carbon nanotube polymer nanocomposites comprising fully aligned SWCNTs. Jack et al. [31] proposed a physics-based computational model to explore the link between the macroscale electrical conductivity and the nanostructure of a dense network made of SWCNTs. Haghgoo et al. [32] examined the piezoresistivity and electrical conductivity of carbon nanotube and graphene nanoplatelets filled with polymer nanocomposites using a 3D Monte Carlo analytical geometrical model. Oskouyi et al. [33] used a Monte Carlo simulation technique to construct a three-dimensional continuum percolation model to explore the percolation behavior of an electrically insulating matrix supplemented with conductive nanoplatelet fillers. Several studies have focused on CNT agglomeration. Liu et al. [34] developed a constant-number direct simulation Monte Carlo model to analyze nanoparticle agglomeration in aqueous suspensions. Gbaguidi et al. [35] investigated a two-dimensional Monte Carlo percolation model for monofiller and hybrid nanocomposites. Deng et al. [36] investigated nanoparticle agglomeration properties using a Monte Carlo simulation. Despite the advantages with inkjet printing of CNT inks and unique microstructures generated, percolation network behavior and electrical conductivity of multilayer inkjet printed films has not been investigated in detail.

In this study, we used a stochastic microstructural model to investigate percolation and electrical conductivity in multilayer printed CNT network structures. We compared the variation in sheet resistance with the number of printed layers produced by our model. Several parametric studies have been conducted to understand the percolation behavior and conductivity of multilayer printing. Microstructures with 0/0° aligned layers were analyzed to investigate the effect of alignment on the resistivity. Parametric studies with varying levels of rope-like and equiaxed agglomeration in multilayer structures were conducted to examine the effect of agglomeration. Finally, experimentally observed microstructures related to sessile drop and twin-line deposition were generated and their conductivity and percolation behaviors were investigated.

III. Model Formulation

We used a quasi-3D continuum percolation model and Monte Carlo simulations to predict the resistance of the CNT ink. CNTs were generated in a cylindrical shape with diameter D_{CNT} in an RVE of length (L_x, L_y, and L_z). The generated CNT is a centerline segment with midpoint (x^i_c, y^i_c, z^i_c), starting point (x^i_1, y^i_1, z^i_1) and ending point (x^i_2, y^i_2, z^i_2) such that:

$$\begin{bmatrix} x^i_2 \\ y^i_2 \\ z^i_2 \end{bmatrix} = \begin{bmatrix} x^i_c \\ y^i_c \\ z^i_c \end{bmatrix} + l^i \begin{bmatrix} \cos\phi^i \\ \sin\phi^i \\ 1 \end{bmatrix} and$$
$$\begin{bmatrix} x^i_1 \\ y^i_1 \\ z^i_1 \end{bmatrix} = \begin{bmatrix} x^i_c \\ y^i_c \\ z^i_c \end{bmatrix} - l^i \begin{bmatrix} \cos\phi^i \\ \sin\phi^i \\ 1 \end{bmatrix} \quad (1)$$

$$\begin{bmatrix} x^i_c \\ y^i_c \\ z^i_c \\ \phi^i \end{bmatrix} = \begin{bmatrix} L_x \times rand^i_1 \\ L_y \times rand^i_2 \\ n \times t \\ 2\pi \times rand^i_3 \end{bmatrix} \quad (2)$$

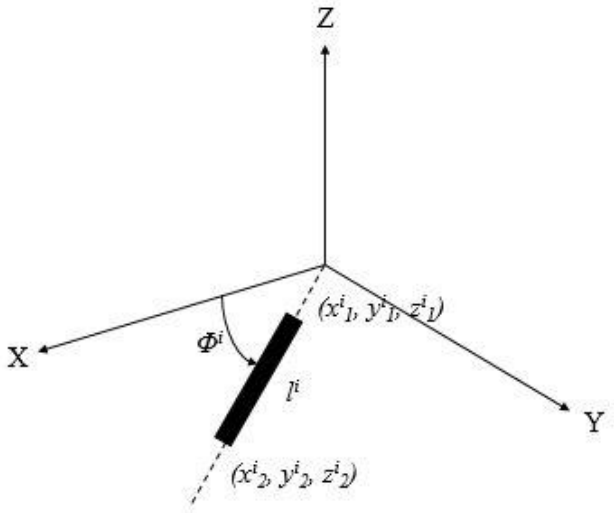

Fig 1. Schematics of line segment of ith CNT.

where l_i, $Ø_i$, n and t are the length, polar angle, number of layers and distance between each layer respectively. CNTs were added to the RVE in each layer until the desired CNT volume fraction was reached. Here, the volume fraction of the CNT is defined as the ratio of the total volume of all CNT ($\pi \times r^i{}_0{}^2 \times l_i$) to the area of the RVE ($L_x \times L_y$) at each layer. From Equation (1) the center of the CNT is always located inside the RVE. However, CNT can intersect with one or two RVE boundaries and in such cases, periodic boundary conditions are applied. Periodic boundary conditions were used to compensate for line segments that are outside the RVE by repositioning the new line segments inside the RVE. A more detailed explanation on generating the CNT microstructure is presented in the reference [35].

The distance between neighboring particles is computed, and if it is smaller than the tunneling cutoff distance (d_{cutoff}), the particles are considered to be electrically connected and form a cluster. The tunneling junction occurs when an electric voltage is applied across the electrode, the electrons in the CNT film can tunnel through the insulating layer and into the electrode [35]. The tunneling effect is observed between the two CNTs when the distance between them is less than the maximum effective distance of tunneling effect. Percolation occurs in the RVE when a cluster links two electrodes (x = 0 and x = L_x), and the resistance of the cluster is calculated. The percolation probability, which is the likelihood that there is at least one conductive route in the RVE crossing two electrodes, is used to evaluate CNT percolation and is given by (3),

$$P = \frac{n_p}{N} \quad (3)$$

In a total of N microstructures, n_p denotes the number of microstructures with at least one conductive path. Figure 2 shows the random microstructure for the number of printed layers equal to 2 and 10. The CNTs are uniformly distributed inside the RVE with agglomeration $\xi_{agg} = 0$. The core premise of Monte Carlo simulation is to employ randomness to solve problems that are predictable in principle [33]. Because we utilize a random microstructure to calculate the desired attributes of the CNT, we must decrease the statistical variance of the properties by averaging across a large number of random microstructures. Based on prior research by Gbaguidi et al. [35], we chose to conduct our simulation for 2000 iterations because the output properties converged around that many iterations. The size of the RVE in our model was kept constant throughout the numerical analysis at 25 μm × 25 μm × (number of layers × thickness) μm.

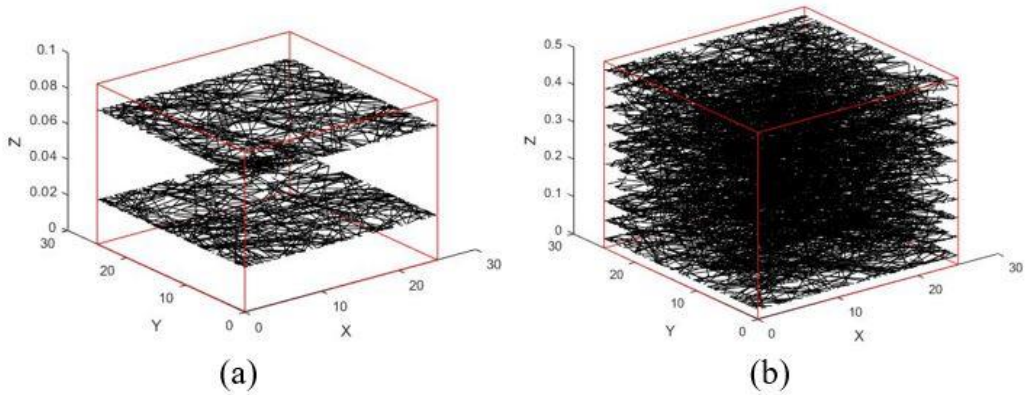

Fig 2. CNT microstructure (a) random orientation of CNT with 2 layers (b) random orientation of CNT with 10 layers.

IV. Results and Discussion

A. Percolation behavior and conductivity of multilayer CNT films

In this section we utilize the model to examine how percolation probability and conductivity of multilayer CNT films varies with changes in the CNT ink composition. For this analysis we model CNTs with a constant length and diameter of 2 μm and 25 nm respectively. CNT microstructures are generated by varying the volume fraction and the number of print layers. The CNT volume fraction for a given ink composition is constant, therefore, we maintained a consistent volume fraction (or area fraction) in each layer for a given multilayer structure. The volume fraction was varied from 0.02 to 0.12, and the number of layers ranged from 2 to 30.

The percolation behavior for the various microstructures as a function of CNT ink composition and number of layers is shown in figure 3. Percolation probability is the likelihood that at least one conductive channel is formed across the two electrodes of the RVE. This is computed using equation (3) discussed in Section 3. About 2000 microstructures with randomly varying CNT network are generated for each combination of input parameters (CNT volume fraction and number of layers). Percolation probability is the ratio of number of microstructures with conductive path compared to the total number of microstructure variations considered.

For two printed layers, percolation occurs with a relatively higher volume fraction of CNT of approximately 0.085, whereas for 30 printed layers, percolation occurs even with a lower volume fraction of 0.03. The percolation threshold decreased as the number of printed layers increased at low CNT volume fractions. When 12 or more layers are modeled, there is a relatively small difference in the ink composition required to achieve percolation. In contrast, higher ink concentration is needed for percolation when fewer number of layers are modeled.

Based on the pattern detected in the percolation probability, it is evident that the conductivity increases with an increase in the number of printed layers, as shown in figure 4. We found that for lower numbers of printed layers (i.e., 2, 4 layers), there is no conductivity until a high-volume percent of CNT is used. However, for higher numbers of printed layers (i.e., 8 and beyond), conductivity is observed starting from a CNT volume fraction of 0.04. The conductivity increases exponentially as the volume fraction of CNT increases. High-density carbon nanotube (CNT) inks with 2-15 wt% was utilized to experimentally fabricate inkjet-printed films with least sheet resistivity of 225 Ω/sq was recorded after printing up to 5 times [37]. Tortorich et al. [38] prepared an aqueous solution containing 0.8 mg/mL of SWCNTs and 3 mg/mL of SDS and the SWCNT ink was printed up to 35 times, reaching a sheet resistance as low as 132 Ω/sq.

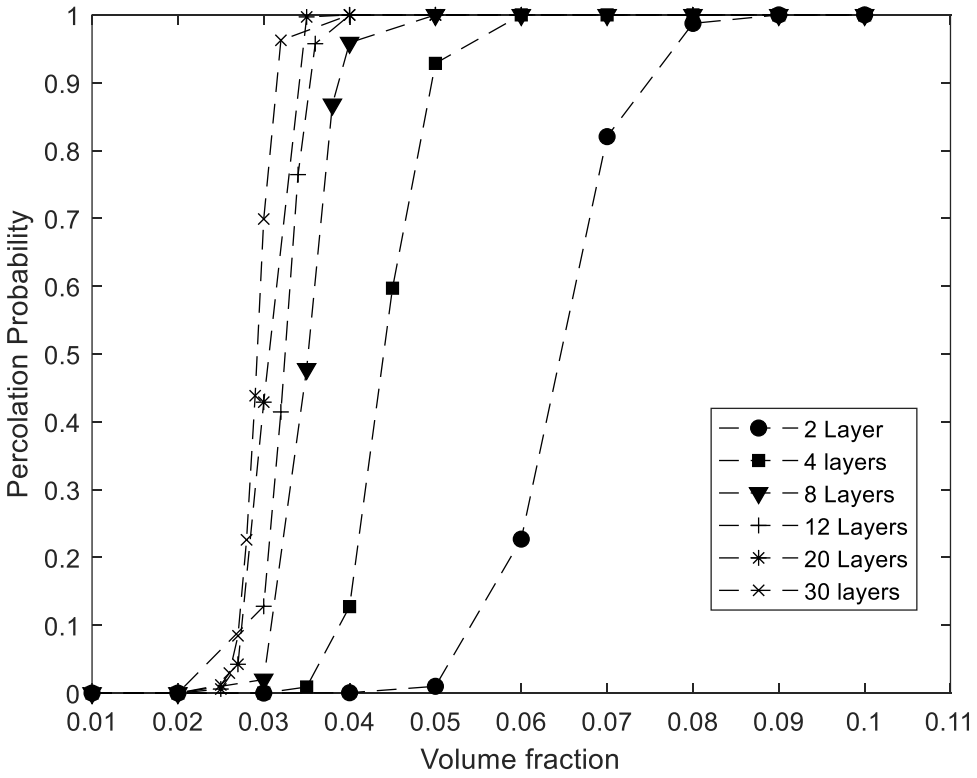

Fig 3. Effect on percolation probability at various volume fraction CNT for multilayer printing.

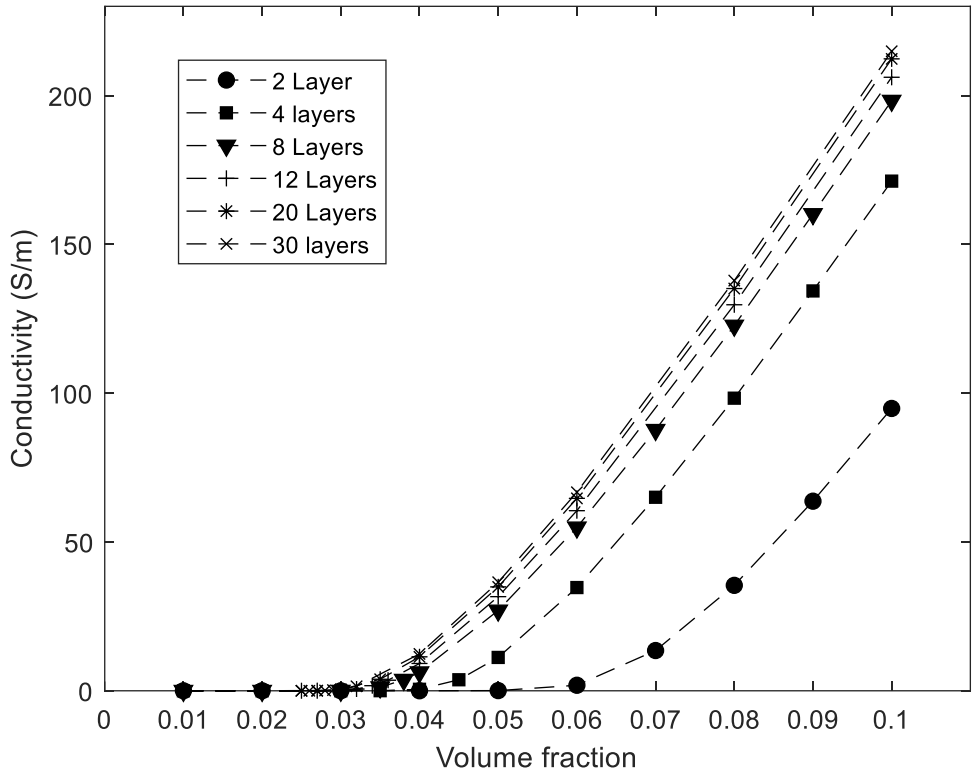

Fig 4. Effect on conductivity at various volume fraction CNT for multilayer printing.

B. Effect of CNT Alignment in multilayer films

Inkjet printing has been used to align carbon nanotubes by several researchers to exhibit improved characteristics [21,22,32]. By rotating the printed substrate, we can get different types of alignment similar to composites plies. Here we examine the effect of alignment in CNT multilayer films.

The aligned microstructures are generated by varying the polar angle (Ø) mentioned in equations 1 and 2. For instance, if the polar angle is fixed at 0° for all CNTs in a given layer, it would produce a perfectly aligned microstructure with parallel CNTs. In a completely random microstructure with no preferential alignment, each nanotube is assigned a random value of polar angle between +90° to -90° with respect to the horizontal axis. Different degrees of alignment can be modeled by restricting the polar angle variation. The degree of alignment is quantified by the limits imposed on the polar angle. For example, figure 5 shows an aligned microstructure with the polar angle variation restricted to 50% of the available range, i.e., between +45° to -45°. Lower variation of polar angle indicates increased alignment. All CNTs are modeled with a constant length and diameter of 2 μm and 25 nm respectively, and a CNT volume fraction of 10% is used in all the microstructures.

Figure 7(a) shows the computations of resistance for the baseline multilayer structure as a function of degree of alignment and number of printed layers. As expected, the resistance is lower for fewer printed layers. The saturation point for percolating paths is reached after 10 print layers. As the alignment is introduced starting from completely random structure (polar angle variation 100%), there is a decrease in resistance indicating an increase in the number of tunneling junctions. This is because the partial alignment of CNTs increases the average path length between the source and drain, resulting in low resistivity. The minima for resistance are observed at 70% polar angle variation as shown in figure 7(b). Increasing the alignment above 70% polar angle variation results in increase in resistance, owing to a reduction in the number of connected pathways between the electrodes. Figure 7(c) shows the percolation probability at various volume fractions of CNT for multilayer printing of 2, 4 and 8 layers. It can be observed that the percolation probability reduces for higher alignments with polar angle variation less than 70%. For highly aligned structures with a polar angle variation less than 30 percent, the resistance was not recorded for less than 10 layers, as percolation could not be reached. Pimparkar et al. [39] studied the alignment performance of nanobundle thin-film transistors. They observed a similar pattern wherein a minor degree of alignment improves the drain current, but near-parallel alignment rapidly lowers the current due to a reduction of connecting pathways.

Rotating the substrate or the print direction can lead to layup configurations similar to composites. We analyze the effect of such configurations by modeling an alternating 0/90° print rotation, in addition to the baseline layered structure. Figure 6 shows two-layer 0/90° microstructures for 10% polar angle variation and 50% polar angle variation. Figure 8(a) shows the resistance of printed microstructures with alternating 0/90° print layers. It can be observed that the resistance with alternating 0/90° configuration is generally lower than 0/0° configuration. This is because the resistance measurement is in the 0° direction. By introducing 90° aligned layers, the number of CNTs forming connections between the source and drain in the 0° direction is reduced. In Figure 8(a), it can be observed that the resistance monotonically increases with the increase in alignment (decreasing polar angle variation). Here we do not observe the parabolic behavior previously observed in 0/0° configurations. In highly aligned structures, presence of 90° intercepting layers creates connections between the CNTs aligned in the 0° direction. This helps in reducing the resistance even for highly aligned structures, Figure 8(b) compares the percolation probabilities for 0/0° and 0/90° configurations. It can be noted that percolation can be attained at lower volume fractions for 0/90° configurations. These results provide a design alternative to address the low drain current experimentally observed in highly aligned structures [39].

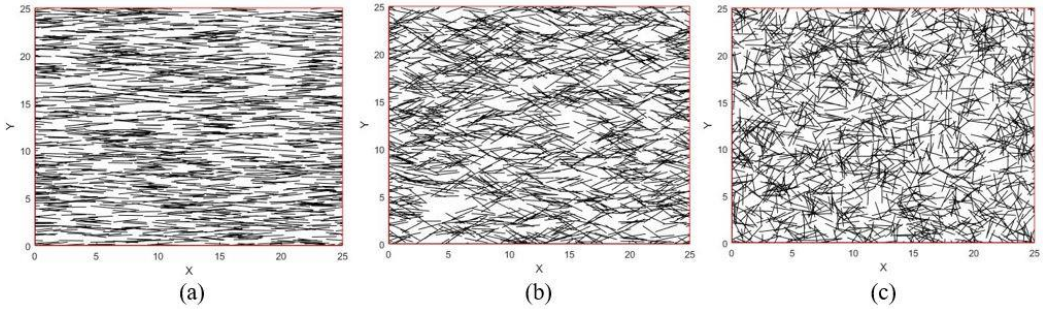

Figure 5. Alignment of CNT for 0/0-degree layer with (a) 10% variation in polar angle (b) 50% variation in polar angle and (c) random orientation.

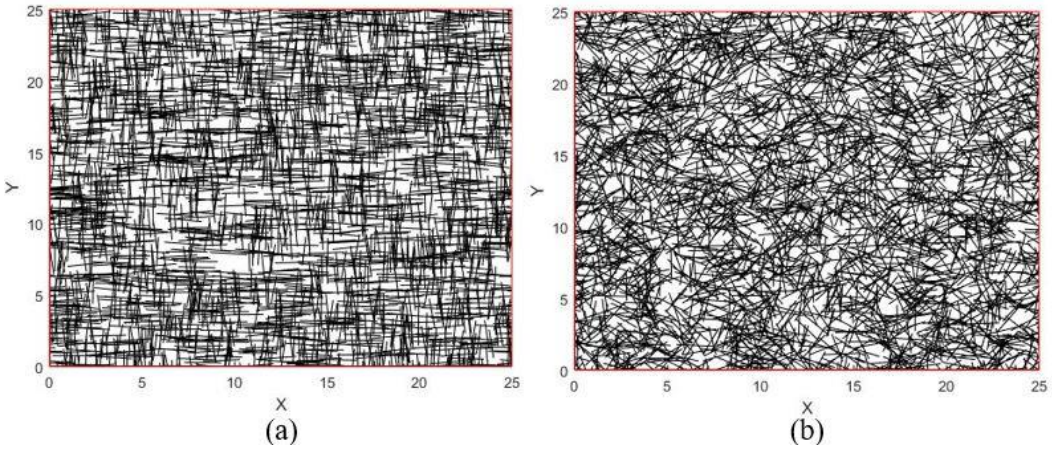

Figure 6. (a) Alignment of CNT 0/90-degree layer with 10% variation in polar angle (b) alignment of CNT 0/90-degree layer with 50% variation in polar angle.

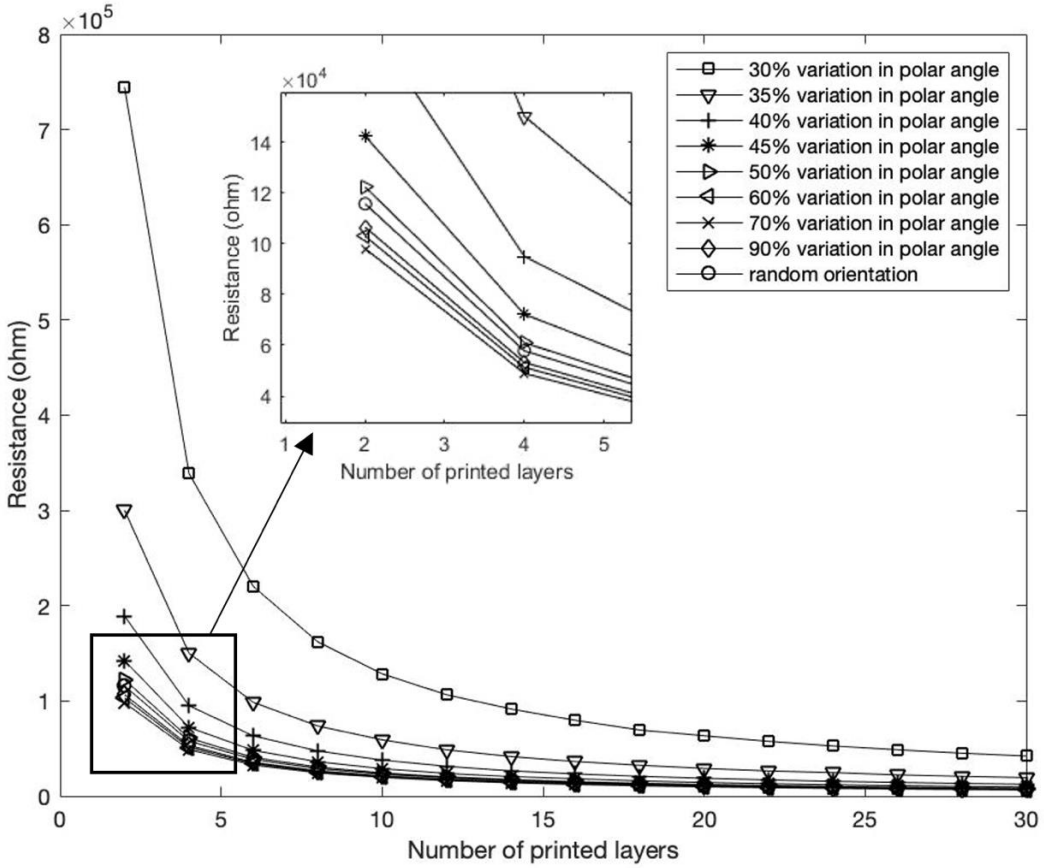

Figure 7(a). Percentage variation of polar angle for 0/0-degree alignment of CNT.

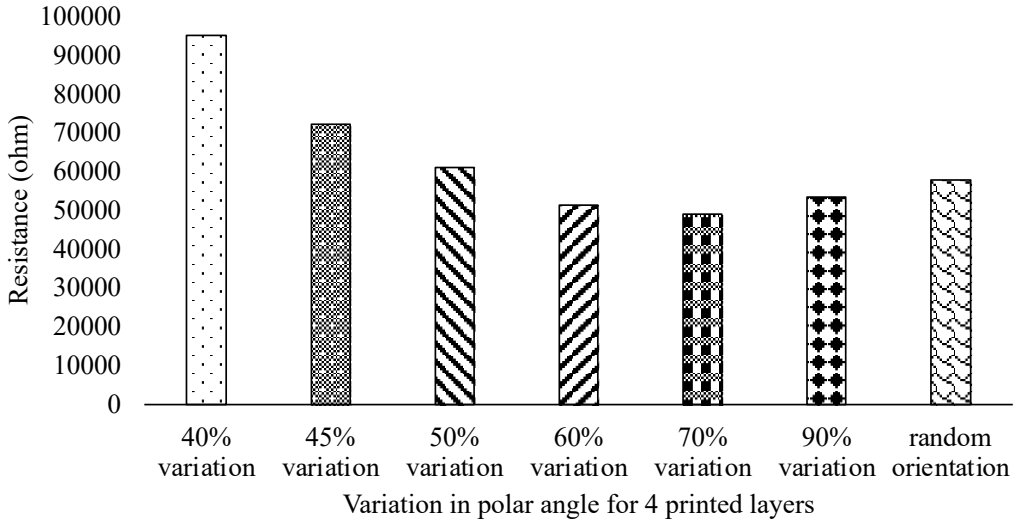

Figure 7(b). Bar chart representation of percentage variation of polar angle for 0/0-degree alignment of CNT.

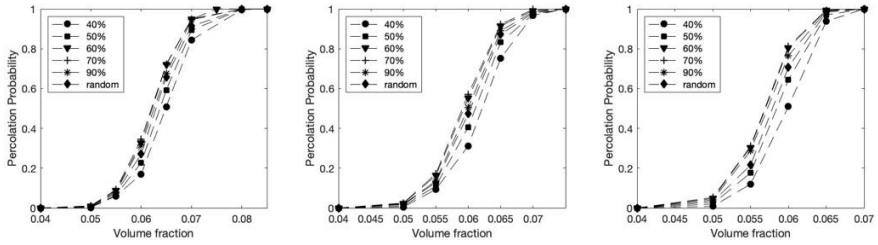

(i) (ii) (iii)

Figure 7(c). Percolation probability at various volume fraction CNT for 0/0-degree alignment of CNT for (i) 2 layers, (ii) 4 layers and (iii) 8 layers printing.

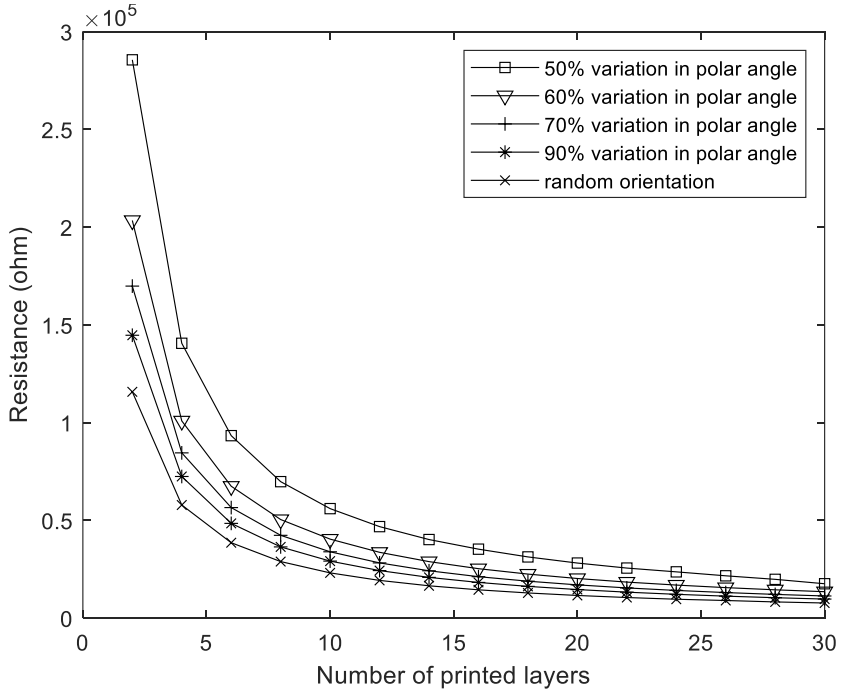

Figure 8(a). Percentage variation of polar angle for 0/90-degree alignment of CNT.

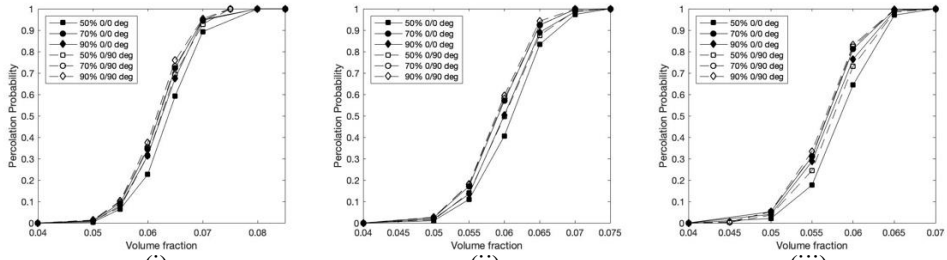

(i) (ii) (iii)

Figure 8(b). Percolation probability comparison at various volume fraction CNT for 0/0 and 0/90-degree alignment of CNT for (i) 2 layers, (ii) 4 layers and (iii) 8 layers printing.

C. Effect of CNT agglomeration in multilayer films

Agglomeration is a common occurrence in printed nanoparticle structures. In this section, we examine the effect of CNT agglomeration in multilayer films. In the literature, agglomerates are characterized as rope-like [40][41], where agglomeration is formed by aligned CNTs, and equiaxed [42][43], where the agglomeration is formed by random CNT orientation.

The rope-like and equiaxed agglomerated microstructures were generated by varying the agglomeration parameter ξ_{agg} and the agglomeration angle α_{agg}. Agglomeration parameter ξ_{agg} defines the percentages of CNTs in agglomerates. When $\xi_{agg} = 0$ then the CNTs are uniformly distributed in the RVE with no agglomeration. As we increase the value of ξ_{agg} the agglomeration level increases. The agglomeration angle α_{agg} determines the variation of the CNT alignment with each other within an agglomerate. When the agglomeration angle $\alpha_{agg} = 0°$, the CNTs in the agglomerates are modeled as parallel to each other resulting in rope-like agglomerates in the microstructure. When the agglomeration angle $\alpha_{agg} = 180°$ equiaxed or star-like agglomerates are generated in the microstructure. Figures 9 (a) and (b) show microstructures with rope-like and equiaxed agglomerates respectively.

A baseline random microstructure is first modeled with $\xi_{agg} = 0$, with CNTs of constant length and diameter of 2 μm and 25 nm respectively, and a CNT volume fraction of 10%. The variation of resistance with increasing number of layers is modeled with this random structure. Subsequently, the change in resistance for increasing agglomeration is modeled for the two cases. Figure 10 shows this variation for rope like agglomerates and figure 11 for equiaxed agglomerates. The resistance increases as the agglomeration level increases. This is because fewer percolation paths are formed for same CNT content when CNTs are agglomerated. Experimental studies have reported that agglomerated microstructures exhibit lower resistance [35]. The model predictions qualitatively align with these observations. We find that rope like agglomerations lead to higher resistance than equiaxed agglomeration for the same agglomeration level and the number of layers. This is because the volume coverage is relatively higher for equiaxed agglomerates compared to rope like structures.

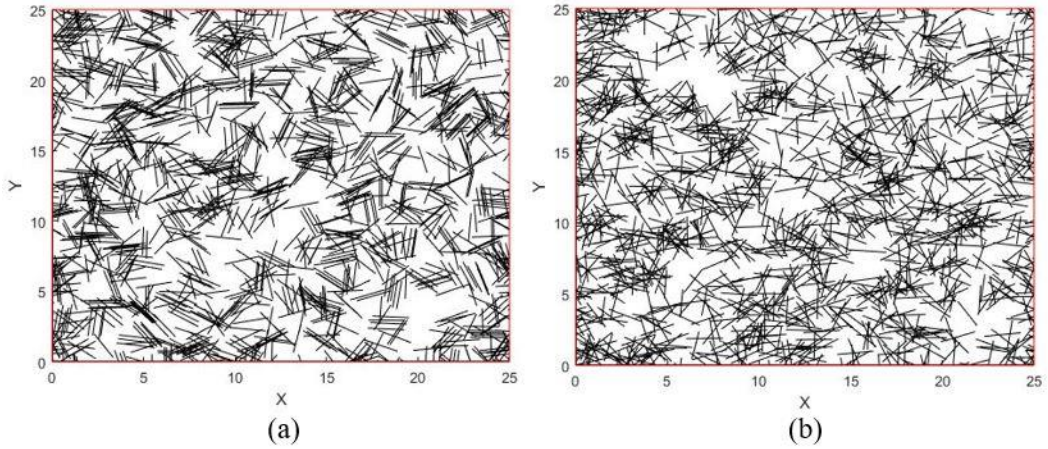

(a) (b)

Fig 9. (a) Rope-like agglomeration microstructure ξagg = 0.70, α = 0° (b) Star-like agglomeration microstructure ξagg = 0.70, α = 180°

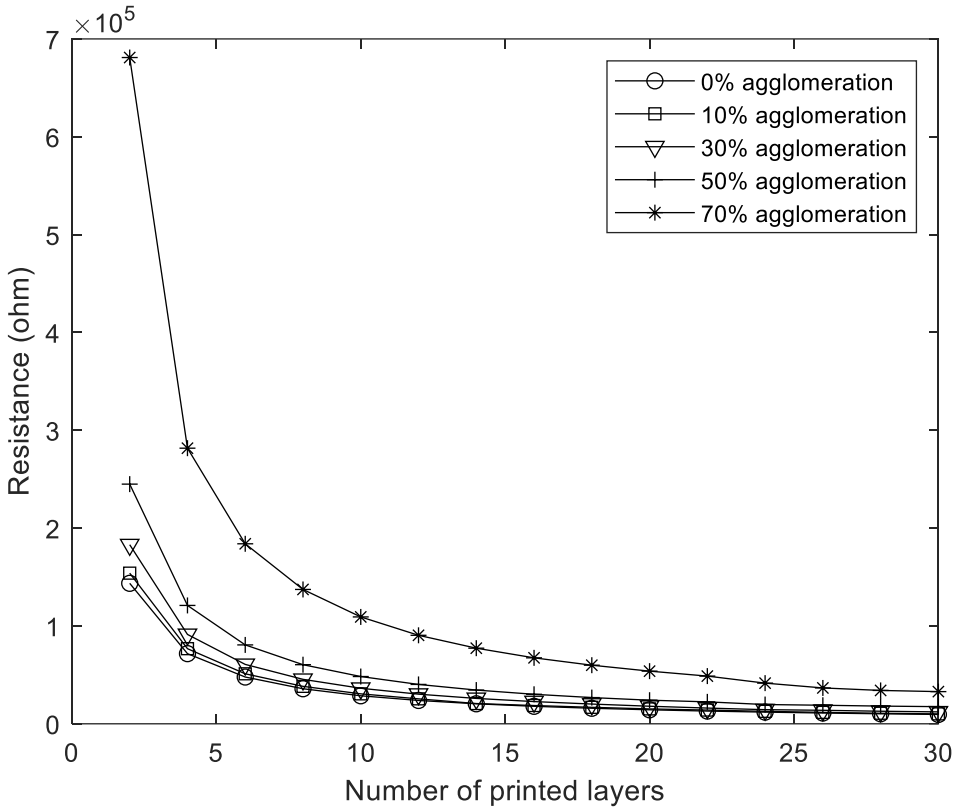

Fig 10. Rope-like agglomeration of CNT.

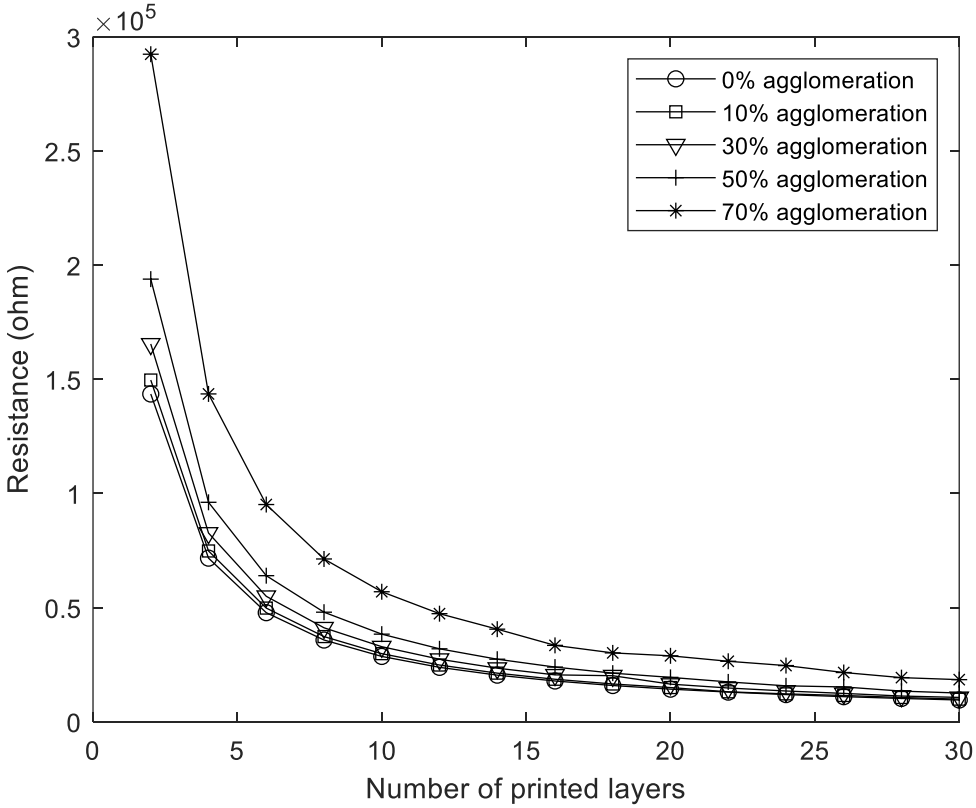

Fig 11. Star-like agglomeration of CNT.

D. Sessile drop and twin-line deposition microstructures

Numerous studies report sessile drop experiments [21][27][28] employing inkjet printing to align CNTs. In the sessile drop experiment, CNT ink is printed on the substrate at the same spot, and simultaneous evaporation is carried out. The evaporation and CNT printing rates are synchronized until the desired volume fraction is achieved. CNTs tend to align along the ink contact line during the evaporation process, producing a coffee ring effect [44][45]. In this section, we model the sessile drop microstructures and study the effect of this feature in multilayer printing. The sessile drop microstructure is modeled by varying the orientation as a function of the position as shown in figure 12.

Similarly, several other studies utilize twin-line deposition approach [17][29][30]. Twin line deposition method uses an inkjet printing where, depending on the drop space in print direction, a twin-line configuration is produced with higher density of nanoparticles at the edges of the print head, and relatively lower particle density in the center. This approach has been used for CNT deposition [21]. In this study, the width of the individual line was 3.3 μm and the distance between the two lines was approximately 6 μm. Approximately 80% of the CNTs lie in the twin-line region, and the remaining 20% lie between the twin-lines. Using these parameters from the literature, the microstructure was generated, as shown in figure 13.

A comparison of the sessile drop and twin-line deposition of the CNT microstructure in terms of the resistivity for multilayer printing is shown in figure 14. The twin-line deposition has a lower resistivity than the sessile drop at lower print layers because, in the twin-line concept, the CNTs are clustered and aligned along the twin-line, forming a highly percolated path compared with the sessile drop concept. At higher print layers (approximately 10 layers), the resistivity trend is similar for both concepts, as it reached the saturation point for percolation. We also compare these microstructures with aligned microstructure from section 4.1. The resistance values for sessile drop and twin line structures are between the microstructures with 30% and 70% polar angle variation.

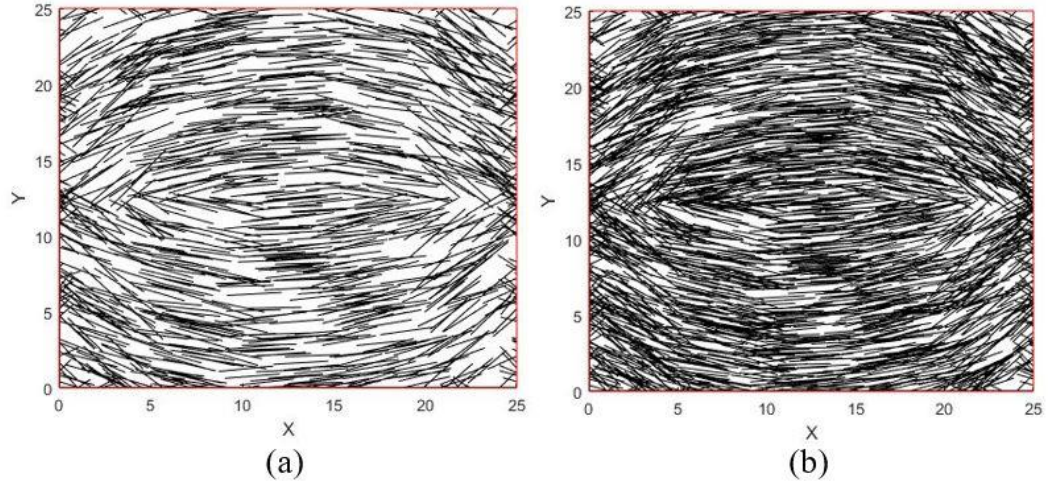

Fig 12. Microstructure of CNT from the literature of sessile drop experiment (a) 1 layer (b) 2 layers.

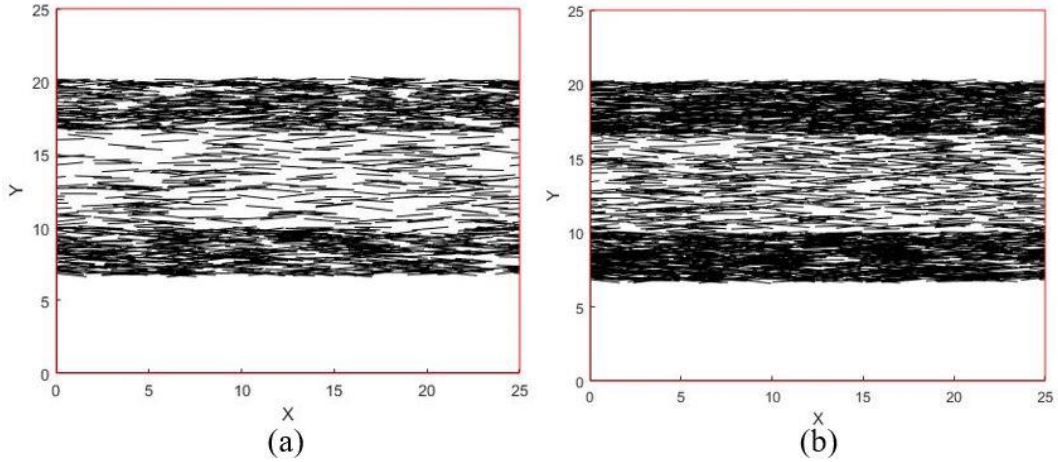

Fig 13. Microstructure of CNT from the literature of twin-line deposition concept (a) 1 layer (b) 2 layers.

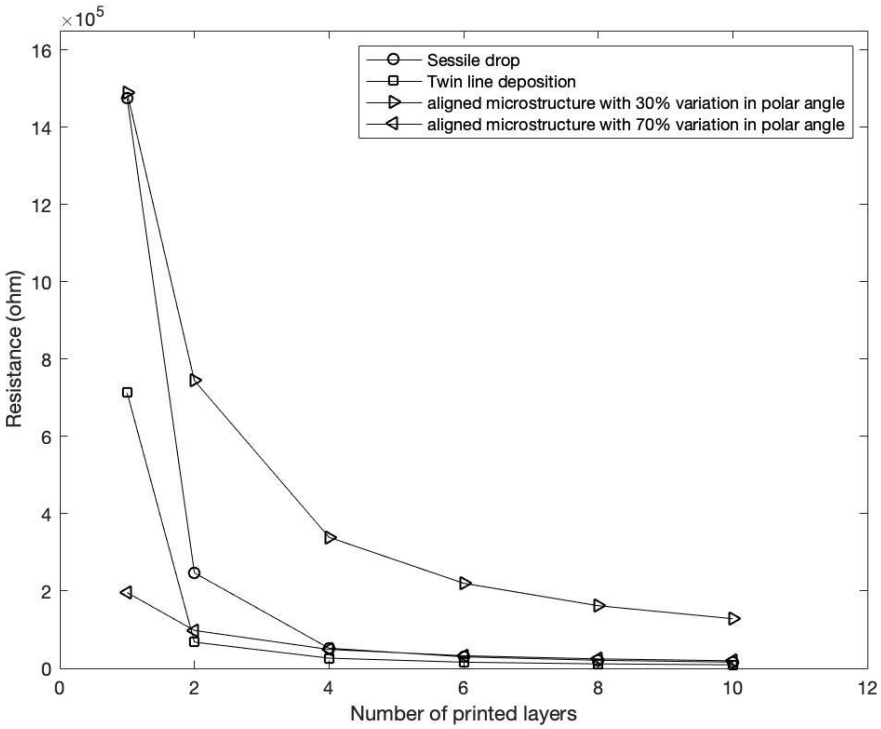

Fig 14. Alignment of CNT microstructure using sessile drop and twin-line deposition concept for multilayer printing comparing with the theoretically aligned microstructure.

V. Conclusion

The stochastic percolation model was used to study the electrical characteristics on inkjet-printed carbon nanotube films. Parametric studies were conducted to analyze the effect of CNT volume fraction, alignment and agglomeration in layer wise printed structures. We note that the conductivity increases with an increase in the number of printed layers. A high CNT volume fraction above 7.5% is needed to generate conductivity for structures with less than 4 printed layers. However, for more than 8 printed layers conductivity is observed starting from a CNT volume fraction of 4%.

Aligned microstructures exhibit a minima in resistivity at 70% polar angle variation. Further alignment reduces the percolation pathways and increases the resistance. Printed microstructures with agglomerates in general resulted in higher resistance compared to microstructures with well dispersed CNTs. Structures with rope like CNT agglomerates exhibit higher resistance than those with equiaxed agglomerates due to the difference in volume coverage. Experimentally observed microstructural configurations like sessile drop and twin line deposition microstructures were also analyzed in this study.

References

[1] Jiang, P., Ji, Z., Zhang, X., Liu, Z., and Wang, X. Recent Advances in Direct Ink Writing of Electronic Components and Functional Devices. *Progress in Additive Manufacturing*. 1–2. Volume 3, 65–86.

[2] Zhang, Y., Jin, Z., and Zhang, W. Application of 3D Printing in Future Manned Space Exploration. No. 982 MSF, 2020, pp. 92–97.

[3] Dunn, J. J., Hutchison, D. N., Kemmer, A. M., Ellsworth, A. Z., Snyder, M., White, W. B., and Blair, B. R. *Space Manufacturing 14: Critical Technologies for Space Settlement-Space Studies Institute 3D Printing in Space: Enabling New Markets and Accelerating the Growth of Orbital Infrastructure*.

[4] Ghidini, T. Regenerative Medicine and 3D Bioprinting for Human Space Exploration and Planet Colonisation. *Journal of Thoracic Disease*. Volume 10, S2363–S2375.

[5] Wong, J. Y., and Pfahnl, A. C. "3D Printing of Surgical Instruments for Long-Duration Space Missions." *Aviation Space and Environmental Medicine*, Vol. 85, No. 7, 2014, pp. 758–763. https://doi.org/10.3357/ASEM.3898.2014.

[6] Terfansky, M. L., and Thangavelu, M. 3D Printing of Food for Space Missions. 2013.
[7] NASA. https://www.nasa.gov/content/open-for-business-3-d-printer-creates-first-object-in-space-on-international-space-station. Accessed Sep. 5, 2023.
[8] Singh, M., Haverinen, H. M., Dhagat, P., and Jabbour, G. E. "Inkjet Printing-Process and Its Applications." *Advanced Materials*, Vol. 22, No. 6, 2010, pp. 673–685. https://doi.org/10.1002/adma.200901141.
[9] Mattana, G., Loi, A., Woytasik, M., Barbaro, M., Noël, V., and Piro, B. "Inkjet-Printing: A New Fabrication Technology for Organic Transistors." *Advanced Materials Technologies*, Vol. 2, No. 10, 2017, pp. 1–27. https://doi.org/10.1002/admt.201700063.
[10] Chang, S. C., Liu, J., Bharathan, J., Yang, Y., Onohara, J., and Kido, J. "Multicolor Organic Light-Emitting Diodes Processed by Hybrid Inkjet Printing." *Advanced Materials*, Vol. 11, No. 9, 1999, pp. 734–737. https://doi.org/10.1002/(SICI)1521-4095(199906)11:9<734::AID-ADMA734>3.0.CO;2-D.
[11] Calvert, P., and Boland, T. "Inkjet Printing of Biopolymers and Cells." No. February, 2019, pp. 1–31.
[12] Karunakaran, S. K., Arumugam, G. M., Yang, W., Ge, S., Khan, S. N., Lin, X., and Yang, G. "Recent Progress in Inkjet-Printed Solar Cells." *Journal of Materials Chemistry A*, Vol. 7, No. 23, 2019, pp. 13873–13902. https://doi.org/10.1039/c9ta03155c.
[13] Han, G. D., Bae, K., Kang, E. H., Choi, H. J., and Shim, J. H. "Inkjet Printing for Manufacturing Solid Oxide Fuel Cells." *ACS Energy Letters*, Vol. 5, No. 5, 2020, pp. 1586–1592. https://doi.org/10.1021/acsenergylett.0c00721.
[14] Müller, K., Bugnicourt, E., Latorre, M., Jorda, M., Echegoyen Sanz, Y., Lagaron, J. M., Miesbauer, O., Bianchin, A., Hankin, S., and Bölz, U. "Review on the Processing and Properties of Polymer Nanocomposites and Nanocoatings and Their Applications in the Packaging, Automotive and Solar Energy Fields." *Nanomaterials*, Vol. 7, No. 4, 2017, p. 74.
[15] Zeng, M., and Zhang, Y. "Colloidal Nanoparticle Inks for Printing Functional Devices: Emerging Trends and Future Prospects." *Journal of Materials Chemistry A*, Vol. 7, No. 41, 2019, pp. 23301–23336. https://doi.org/10.1039/c9ta07552f.
[16] Kao, H. L., Cho, C. L., Chang, L. C., Chen, C. B., Chung, W. H., and Tsai, Y. C. "A Fully Inkjet-Printed Strain Sensor Based on Carbon Nanotubes." *Coatings*, Vol. 10, No. 8, 2020. https://doi.org/10.3390/COATINGS10080792.
[17] Dinh, N. T., Sowade, E., Blaudeck, T., Hermann, S., Rodriguez, R. D., Zahn, D. R. T., Schulz, S. E., Baumann, R. R., and Kanoun, O. "High-Resolution Inkjet Printing of Conductive Carbon Nanotube Twin Lines Utilizing Evaporation-Driven Self-Assembly." *Carbon*, Vol. 96, 2016, pp. 382–393. https://doi.org/10.1016/j.carbon.2015.09.072.
[18] Ko, H., and Tsukruk, V. V. "Liquid-Crystalline Processing of Highly Oriented Carbon Nanotube Arrays for Thin-Film Transistors." *Nano Letters*, Vol. 6, No. 7, 2006, pp. 1443–1448. https://doi.org/10.1021/nl060608r.
[19] Wang, Q., Yao, Q., Chang, J., and Chen, L. "Enhanced Thermoelectric Properties of CNT/PANI Composite Nanofibers by Highly Orienting the Arrangement of Polymer Chains." *Journal of Materials Chemistry*, Vol. 22, No. 34, 2012, pp. 17612–17618. https://doi.org/10.1039/c2jm32750c.
[20] Lim, J. H., Phiboolsirichit, N., Mubeen, S., Rheem, Y., Deshusses, M. A., Mulchandani, A., and Myung, N. V. "Electrical and Sensing Properties of Single-Walled Carbon Nanotubes Network: Effect of Alignment and Selective Breakdown." *Electroanalysis*, Vol. 22, No. 1, 2010, pp. 99–105. https://doi.org/10.1002/elan.200900314.
[21] Goh, G. L., Saengchairat, N., Agarwala, S., Yeong, W. Y., and Tran, T. "Sessile Droplets Containing Carbon Nanotubes: A Study of Evaporation Dynamics and CNT Alignment for Printed Electronics." *Nanoscale*, Vol. 11, No. 22, 2019, pp. 10603–10614. https://doi.org/10.1039/c9nr03261d.
[22] Goh, G. L., Agarwala, S., and Yeong, W. Y. "Directed and On-Demand Alignment of Carbon Nanotube: A Review toward 3D Printing of Electronics." *Advanced Materials Interfaces*, Vol. 6, No. 4, 2019. https://doi.org/10.1002/admi.201801318.
[23] Beyer, S. T., and Walus, K. "Controlled Orientation and Alignment in Films of Single-Walled Carbon Nanotubes Using Inkjet Printing." *Langmuir*, Vol. 28, No. 23, 2012, pp. 8753–8759. https://doi.org/10.1021/la300770b.
[24] Beard, J. D., Stringer, J., Ghita, O. R., and Smith, P. J. "High Yield Growth of Patterned Vertically Aligned Carbon Nanotubes Using Inkjet-Printed Catalyst." *ACS Applied Materials and Interfaces*, Vol. 5, No. 19, 2013, pp. 9785–9790. https://doi.org/10.1021/am402942q.
[25] Li, Q., Zhu, Y. T., Kinloch, I. A., and Windle, A. H. "Self-Organization of Carbon Nanotubes in Evaporating Droplets." *Journal of Physical Chemistry B*, Vol. 110, No. 28, 2006, pp. 13926–13930. https://doi.org/10.1021/jp061554c.

[26] Zhang, S., Li, Q., Kinloch, I. A., and Windle, A. H. "Ordering in a Droplet of an Aqueous Suspension of Single-Wall Carbon Nanotubes on a Solid Substrate." *Langmuir*, Vol. 26, No. 3, 2010, pp. 2107–2112. https://doi.org/10.1021/la902642f.

[27] Small, W. R., Walton, C. D., Loos, J., and In Het Panhuis, M. "Carbon Nanotube Network Formation from Evaporating Sessile Drops." *Journal of Physical Chemistry B*, Vol. 110, No. 26, 2006, pp. 13029–13036. https://doi.org/10.1021/jp062365x.

[28] Bromberg, V., Ma, S., and Singler, T. J. "High-Resolution Inkjet Printing of Electrically Conducting Lines of Silver Nanoparticles by Edge-Enhanced Twin-Line Deposition." *Applied Physics Letters*, Vol. 102, No. 21, 2013. https://doi.org/10.1063/1.4807782.

[29] Takagi, Y., Nobusa, Y., Gocho, S., Kudou, H., Yanagi, K., Kataura, H., and Takenobu, T. "Inkjet Printing of Aligned Single-Walled Carbon-Nanotube Thin Films." *Applied Physics Letters*, Vol. 102, No. 14, 2013. https://doi.org/10.1063/1.4801496.

[30] Puydupin-Jamin, A. S., and Seidel, G. D. "Computational Micromechanics Analysis of the Effects of Bundle Packing and Interphase Addition on the Effective Electrical and Thermal Transverse Conductivity of Carbon Nanotube-Polymer Nanocomposites." *Collection of Technical Papers - AIAA/ASME/ASCE/AHS/ASC Structures, Structural Dynamics and Materials Conference*, No. April, 2010. https://doi.org/10.2514/6.2010-2523.

[31] Jack, D. A., Yeh, C. S., Liang, Z., Li, S., Park, J. G., and Fielding, J. C. "Electrical Conductivity Modeling and Experimental Study of Densely Packed SWCNT Networks." *Nanotechnology*, Vol. 21, No. 19, 2010. https://doi.org/10.1088/0957-4484/21/19/195703.

[32] Haghgoo, M., Ansari, R., and Hassanzadeh-Aghdam, M. K. "Monte Carlo Analytical-Geometrical Simulation of Piezoresistivity and Electrical Conductivity of Polymeric Nanocomposites Filled with Hybrid Carbon Nanotubes/Graphene Nanoplatelets." *Composites Part A: Applied Science and Manufacturing*, Vol. 152, No. November 2021, 2022, p. 106716. https://doi.org/10.1016/j.compositesa.2021.106716.

[33] Oskouyi, A. B., Sundararaj, U., and Mertiny, P. "Tunneling Conductivity and Piezoresistivity of Composites Containing Randomly Dispersed Conductive Nano-Platelets." *Materials*, Vol. 7, No. 4, 2014, pp. 2501–2521. https://doi.org/10.3390/ma7042501.

[34] Liu, H. H., Surawanvijit, S., Rallo, R., Orkoulas, G., and Cohen, Y. "Analysis of Nanoparticle Agglomeration in Aqueous Suspensions via Constant-Number Monte Carlo Simulation." *Environmental Science and Technology*, Vol. 45, No. 21, 2011, pp. 9284–9292. https://doi.org/10.1021/es202134p.

[35] Gbaguidi, A., Namilae, S., and Kim, D. "Stochastic Percolation Model for the Effect of Nanotube Agglomeration on the Conductivity and Piezoresistivity of Hybrid Nanocomposites." *Computational Materials Science*, Vol. 166, 2019, pp. 9–19.

[36] Deng, X., Huang, Z., Wang, W., and Davé, R. N. "Investigation of Nanoparticle Agglomerates Properties Using Monte Carlo Simulations." *Advanced Powder Technology*, Vol. 27, No. 5, 2016, pp. 1971–1979. https://doi.org/10.1016/j.apt.2016.06.029.

[37] Denneulin, A., Bras, J., Blayo, A., Khelifi, B., Roussel-Dherbey, F., and Neuman, C. "The Influence of Carbon Nanotubes in Inkjet Printing of Conductive Polymer Suspensions." *Nanotechnology*, Vol. 20, No. 38, 2009. https://doi.org/10.1088/0957-4484/20/38/385701.

[38] Tortorich, R. P., Song, E., and Choi, J.-W. "Inkjet-Printed Carbon Nanotube Electrodes with Low Sheet Resistance for Electrochemical Sensor Applications." *Journal of The Electrochemical Society*, Vol. 161, No. 2, 2014, pp. B3044–B3048. https://doi.org/10.1149/2.008402jes.

[39] Ibrahim, N., Akindoyo, J. O., and Mariatti, M. Recent Development in Silver-Based Ink for Flexible Electronics. *Journal of Science: Advanced Materials and Devices*. 1. Volume 7.

[40] Kanoun, O., Bouhamed, A., Ramalingame, R., Bautista-Quijano, J. R., Rajendran, D., and Al-Hamry, A. Review on Conductive Polymer/CNTs Nanocomposites Based Flexible and Stretchable Strain and Pressure Sensors. *Sensors*. 2. Volume 21, 1–29.

[41] Rafiq, M., Khan, R. S., Rather, A. H., Wani, T. U., Qureashi, A., Pandith, A. H., Rather, S. ullah, and Sheikh, F. A. Overview of Printable Nanoparticles through Inkjet Process: Their Application towards Medical Use. *Microelectronic Engineering*. Volume 266.

[42] Pimparkar, N., Kocabas, C., Kang, S. J., Rogers, J., and Alam, M. A. "Limits of Performance Gain of Aligned CNT over Randomized Network: Theoretical Predictions and Experimental Validation." *IEEE Electron Device Letters*, Vol. 28, No. 7, 2007, pp. 593–595. https://doi.org/10.1109/LED.2007.898256.

[43] Jarali, C. S., Patil, S. F., and Pilli, S. C. "Hygro-Thermo-Electric Properties of Carbon Nanotube Epoxy Nanocomposites with Agglomeration Effects." *Mechanics of Advanced Materials and Structures*, Vol. 22, No. 6, 2015, pp. 428–439. https://doi.org/10.1080/15376494.2013.769654.

[44] Prakash, N., and Seidel, G. D. "Electromechanical Peridynamics Modeling of Piezoresistive Response of Carbon Nanotube Nanocomposites." *Computational Materials Science*, Vol. 113, 2016, pp. 154–170. https://doi.org/10.1016/j.commatsci.2015.11.008.

[45] Ma, P.-C., Siddiqui, N. A., Marom, G., and Kim, J.-K. "Dispersion and Functionalization of Carbon Nanotubes for Polymer-Based Nanocomposites: A Review." *Composites Part A: Applied Science and Manufacturing*, Vol. 41, No. 10, 2010, pp. 1345–1367.